



HAL
open science

VHH characterization. Comparison of recombinant with chemically synthesized anti-HER2 VHH

Lucie Hartmann, Thomas Botzanowski, Mathieu Galibert, Magali Jullian, Eric Chabrol, Gabrielle Zeder-lutz, Valerie Kugler, Johann Stojko, Jean-marc Strub, Gilles Ferry, et al.

► To cite this version:

Lucie Hartmann, Thomas Botzanowski, Mathieu Galibert, Magali Jullian, Eric Chabrol, et al.. VHH characterization. Comparison of recombinant with chemically synthesized anti-HER2 VHH. *Protein Science*, 2019, 28 (10), pp.1865-1879. 10.1002/pro.3712 . hal-02341567

HAL Id: hal-02341567

<https://hal.science/hal-02341567>

Submitted on 15 Sep 2020

HAL is a multi-disciplinary open access archive for the deposit and dissemination of scientific research documents, whether they are published or not. The documents may come from teaching and research institutions in France or abroad, or from public or private research centers.

L'archive ouverte pluridisciplinaire **HAL**, est destinée au dépôt et à la diffusion de documents scientifiques de niveau recherche, publiés ou non, émanant des établissements d'enseignement et de recherche français ou étrangers, des laboratoires publics ou privés.



VHH characterization. Comparison of recombinant and the chemically synthesized anti-HER2 VHH.

Journal:	<i>Protein Science</i>
Manuscript ID	PRO-19-0170.R1
Wiley - Manuscript type:	Full-Length Papers
Date Submitted by the Author:	n/a
Complete List of Authors:	<p>Hartmann, Lucie; Université de Strasbourg, Plateforme IMPReSs, Laboratoire de Biotechnologie et Signalisation Cellulaire Botzanowski, Thomas; IPHC, BioOrganic Mass Spectrometry Laboratory (LSMBO) Galibert, Mathieu; Genepep SA Jullian, Magali; Genepep SA Chabrol, Eric; Institut de recherches SERVIER, Biotechnologies, Pharmacologie Moléculaire et Cellulaire Zeder-Lutz, Gabrielle; Université de Strasbourg, Plateforme IMPReSs, Laboratoire de Biotechnologie et Signalisation Cellulaire Kugler, Valerie; Université de Strasbourg, Plateforme IMPReSs, Laboratoire de Biotechnologie et Signalisation Cellulaire Stojko, Johann; Institut de recherches SERVIER, Biotechnologies, Pharmacologie Moléculaire et Cellulaire Strub, Jean-Marc; IPHC, BioOrganic Mass Spectrometry Laboratory (LSMBO) Ferry, Gilles; Institut de recherches SERVIER, Biotechnologies, Pharmacologie Moléculaire et Cellulaire Frankiewicz, Lukasz; Genepep SA Puget, Karine; Genepep SA Wagner, Renaud; Université de Strasbourg, Plateforme IMPReSs, Laboratoire de Biotechnologie et Signalisation Cellulaire Cianférani, Sarah; IPHC, BioOrganic Mass Spectrometry Laboratory (LSMBO) Boutin, Jean; Institut de recherches SERVIER, Biotechnologies, Pharmacologie Moléculaire et Cellulaire</p>
Keywords:	VHH, expression, chemical synthesis, characterization, structure, affinity, mass spectrometry ion mobility, surface plasmon resonance

1 **VHH characterization.**
2 **Comparison of recombinant and the chemically synthesized anti-HER2 VHH.**

3
4
5 Lucie Hartmann^{1#}, Thomas Botzanowski^{2#}, Mathieu Galibert^{3#}, Magali Jullian³, Eric Chabrol⁴,
6 Gabrielle Zeder-Lutz¹, Valérie Kugler¹, Johann Stojko⁴, Jean-Marc Strub², Gilles Ferry⁴,
7 Lukasz Frankiewicz³, Karine Puget³, Renaud Wagner¹, Sarah Cianférani², Jean A. Boutin^{5,*}

8
9
10 ¹ Plateforme IMPReSs, Laboratoire de Biotechnologie et Signalisation Cellulaire, CNRS, Université
11 de Strasbourg, Illkirch, France

12 ² Laboratoire de Spectrométrie de Masse BioOrganique, Université de Strasbourg, CNRS, IPHC UMR
13 67178, Strasbourg, France

14 ³ Genepep SA. Saint Jean de Védas, France

15 ⁴ Institut de Recherches Servier, Croissy-sur-Seine, France

16 ⁵ Institut de Recherches Internationales Servier, Suresnes, France

17

18 # These three authors contributed equally to the work.

19 * To whom correspondence should be addressed: Dr. JA Boutin, Institut de Recherches Internationales
20 Servier, 50 rue Carnot, 92284 Suresnes Cedex, France. Email : jean.boutin@servier.com; phone :
21 +33155724400

22

23 **Running title:** Synthetic VHH comparative characterization

24 **Total number of manuscript pages:** 29

25 **Tables:** 5

26 **Figures:** 9

27

28

29 **Abstract**

30 In the continuous exploration of the VHH chemistry, biochemistry and therapeutic future use, we
31 investigated two different production strategies of this small antibody-like protein, using an anti-HER2
32 VHH as a model. The total chemical synthesis of the 125 amino-acid peptide was performed with
33 reasonable yield, even if optimization will be necessary to upgrade this kind of production. In parallel,
34 we expressed the same sequence in two different hosts: *E. coli* and *P. pastoris*. Both productions were
35 successful and led to a fair amount of VHHs. The integrity and conformation of the VHH were
36 characterized by complementary mass spectrometry approaches, while surface plasmon resonance
37 experiments were used to assess the VHH recognition capacity and affinity towards its “antigen”.
38 Using this combination of orthogonal techniques, it was possible to show that the 3 VHHs – whether
39 synthetic or recombinant ones – were properly and similarly folded and recognized the “antigen”
40 HER2 with similar affinities, in the nanomolar range. This opens a route towards further exploration
41 of modified VHH with unnatural aminoacids and subsequently, VHH-drug conjugates.

42
43 **Keywords:** VHH, HER2, expression, chemical synthesis, native chemical ligation, affinity,
44 characterization, mass spectrometry, ion-mobility, surface plasmon resonance

45

46

47 **Introduction**

48

49

50

51

52

53

54

55

56

57

58

59

60

61

62

63

64

65

66

67

68

69

70

71

72

73

74

75

76

77

78

79

80

81

82

In the therapeutic area, a paradigm shift had occurred these last years: from an almost-all small molecule approach to drug, there has been a shift and an increasing interest for bigger objects united under the name of Biologics. Among them, and away from the nucleotide-derived approaches, such as miR¹, antisense² and siRNA³, there have been essentially cells such as stem cells⁴ and proteins. Proteins have been used for more than a decade as substitutes of defective naturally-produced ones such as insulin⁵ or EGF. It became increasingly obvious that antibody therapy⁶ might afford new tools to fight major diseases such as cancer⁷. One of the main obstacles to the use of cytotoxic small molecules is the lack of specificity of those compounds towards cancer cells, leading to the well-known side effects. A way to circumvent this lack of specificity is to address the compounds to the diseased cells, thanks to the use of antibodies raised specifically towards a target overexpressed in those cancer cells such as PD1, HER2, etc. The notion of antibody-drug conjugates was born...

The next problems were thus a/ to attach cytotoxic compounds to the antibodies – that acts like cargos – in a reliable and reproductive way and b/ to produce this material to an industrial scale. The cost of this last item became a priority and a source of concern, as antibody-based therapies might rapidly skyrocket, such as cell-based ones. These facts nourished our immediate reflections on how to maintain the specificity and accessibility while gaining in terms of productivity and cost.

Camelids and sharks have surprisingly something in common: the way their antibody system is designed⁸. Indeed, besides the classical double-chain antibodies, shared by all living animals, they also have single-chain ones. Even more interesting is the fact that the variable portion of their heavy chain bears the full antigen-recognition site. This portion of the protein can be isolated as a single, rather short polypeptide while the antigen recognition potency is maintained. In other words, this approach can provide protein scaffolds far smaller than full antibodies (12 kDa versus 150 kDa) or conventional antibody fragments (about 55 kDa for a Fab). They present immediate interest in term of production cost, but also in term of mastering their expression as well as their modification. The antibody fragments derived from camelids single-chain antibodies were named VHHs or nanobodies⁹. Many were raised *versus* several recognized target proteins, such as albumin, EGF receptor, PD1, HER2, etc. They obviously offer new possibilities in many therapeutic areas¹⁰.

Other types of proteins that have the possibility to specifically interact with a given target to form strong complexes have been described¹¹. *À la façon* of the antibody/antigen complex, they present a high level of specificity and fair levels of avidity. We saw in this area the possibility to develop a strategy by which the scaffold would be synthesized chemically, permitting the introduction in the sequence of one or several exotic amino acids. We applied those approaches to several proteins (ubiquitin¹² or an enzyme: calstabin¹³) and were interested to extend this strategy to VHHs. Indeed, the size of those proteins permitted to anticipate two things: a/ the feasibility of their production by

83 recombinant host(s) and b/ the possibility to reach those structures by a total chemical synthesis, even
84 at an industrial scale. The possibility to access the introduction of exotic amino acids in a given
85 sequence would open a new way to introduce new chemical functions that would be easily and
86 specifically alkylated with cytotoxic compound(s) (or other, including fluorophore, for example)
87 bearing the *ad hoc* chemical function (see review by Kent¹⁴).

88 The next step is to explore the possibility to either express a model VHH in two different hosts
89 (*E. coli* and *P. pastoris*) or to chemically produce it. Once the proteins were purified and characterized
90 for their structure, we measured their affinities towards their antigen, HER2. The three proteins
91 behaved in a similar way, opening an avenue of possibilities for future trends in this area, in particular
92 with the possibility to include exotic amino acids that would permit to introduce new chemistry
93 approaches, orthogonal to the classical peptide chemistry, leading to endless possibilities to build new
94 entities such as armed VHHs for a more targeted delivery of cytotoxic molecules, for example.

95

96

97

98 Results

99

100 Expression of anti-HER2 VHH by *Escherichia coli*

101 The genetic construct was transformed in *E. coli Shuffle T7 express* strain for the anti-HER2 VHH
102 cytoplasmic expression. The protein was purified in a conventional manner, through a nickel-affinity
103 chromatography step, followed by a cation exchange chromatography. The anti-HER2 VHH was
104 produced in high quantity — in the 100 mg/L range — and in the correct oxidation state. As can be
105 seen from **Figure 1 (lane Ec)**, the VHH runs to the right molecular weight and seems to be fairly pure.
106 Of course, minute information on the homogeneity of the preparations cannot be extrapolated from
107 such an SDS-PAGE gel, and only further characterization will be able to detail the quality of the VHH
108 polypeptide.

109

110 Expression of a secreted anti-HER2 VHH using *Pichia pastoris* yeast

111 The anti-HER2 VHH construct was introduced into *P. pastoris* by electroporation. Since the resulting
112 yeast transformants potentially bear a variable number of plasmid copies integrated into their genome,
113 isolated clones were then screened in a 96-wells plate format for their performance in producing the
114 recombinant VHH. Dot-blot and Western-blot immunodetection assays performed on the culture
115 supernatants thus led to the selection of the clone secreting the highest amounts of the anti-HER2
116 VHH (**not shown**) This clone was further used for the production step, whereby the VHH was directly
117 purified from the culture supernatant with a single IMAC purification. A final concentration step
118 eventually led to the recovery of about 10 mg of anti-HER2 VHH per liter of yeast culture, with a high
119 degree of purity (**Figure 1, lane Pp**).

120

121 Chemical synthesis of anti-HER2 VHH

122 The synthesis strategy for preparing VHH entailed three peptide segments (F1, F2 and F3, see **Figure**
123 **2**). Due to the lack of solubility of the peptide F1, this segment was modified on Gly9 with a
124 removable backbone linker. An hexahistidine tag was attached to the modification group (RMBO)
125 using Fmoc solid phase peptide synthesis (SPPS)¹⁵. This tag increased the solubility of the fragment
126 and facilitated the purification process with nickel affinity column¹⁶. Peptides F1 and F2 were
127 prepared as peptide hydrazides for subsequent *in situ* activation/thiolysis for native chemical ligation
128 (NCL)¹⁷, while the peptide F3 was prepared with a C-terminal carboxylic acid. The first ligation
129 reaction, F1 to F2 at the Ser21-Cys22 junction, was completed in 16 h and the ligation product F1-2
130 was then purified by HPLC and affinity column. F1-2 was then ligated to F3 to obtain the full length
131 VHH. The His-tag was then removed under TFA treatment and purified on affinity chromatography
132 column. The peptide was then folded and purified by HPLC yielding the pure protein. They were
133 individually purified and analyzed by ESI-MS (**Figure 3**). The resuspension of the lyophilized powder

134 in an aqueous Tris buffer containing 5 % DMSO (**Figure 1, lane synth**) enabled to increase its
135 solubility from 5 % to 18 % compared to a buffer without DMSO. The major part of the VHH remains
136 though insoluble, which might be improved with adjustments of the last purification steps and
137 lyophilization procedure.

138

139 **Mass spectrometry characterization of VHH constructs**

140 We have used mass spectrometry based-methods in order to compare the anti-HER2 VHH obtained
141 from the three production systems

142 *Purity and homogeneity/heterogeneity assessment of anti-HER2 VHH products by LC-UV-MS and*
143 *native MS.* We first assessed the purity and homogeneity/heterogeneity of each anti-HER2 VHH
144 (detailed protein sequences are provided in **Table 1**) product using reversed phase HPLC-MS (**Figure**
145 **4**). LC-UV-MS analysis of the synthetic VHH sample revealed a highly homogeneous sample with
146 only one main peak detected corresponding to the fully oxidized S-S form of the VHH (14022.7 ± 0.3
147 Da, expected mass 14022.6 Da, see **Table 2**). LC-MS analysis of *P. pastoris* VHH revealed a slightly
148 more heterogeneous sample with only two main peaks observed by LC-UV corresponding to oxidized
149 S-S (retention time 13.5 min, 14166.9 ± 0.5 Da, theoretical mass 14166.7 Da) and the reduced SH
150 forms (rt 14.9 min, 14168.9 ± 0.4 Da, theoretical mass 14168.7 Da) with a ratio of 62/38, respectively.
151 Conversely, LC-MS analysis of *E. coli* VHH revealed a highly heterogeneous sample with two main
152 clusters of peaks detected. The first main cluster (~15.3 min) could be attributed to *E. coli* anti-HER2
153 VHH oxidized S-S forms (as a mixture of intact - 14153.9 ± 0.3 Da - and C-terminal truncated -
154 13605.4 ± 0.2 Da forms - , while expected masses were 14153.8 Da and 13605.2 Da, respectively).
155 The second cluster (~16.6 min) corresponds to reduced SH forms (14155.9 ± 0.5 Da and 13607.6 ± 0.4
156 Da, expected masses 14155.8 Da and 13607.2 Da, respectively) of a disulfide bridge formed between
157 Cys23 and Cys96 (only two cysteines are in the VHH sequence). Interestingly, this S-S bridge is not
158 universal among the described VHHs, some of them do not have this feature, rendering it not
159 completely canonical in this context. Of note, a third minor cluster of peaks could be detected at ~17.4
160 min with a mass increase of +28 Da on both intact and C-terminal truncated anti-HER2 VHH forms
161 (14183.9 ± 0.2 Da and 13635.5 ± 0.4 Da, expected masses 14183.9 Da and 13635.2 Da, respectively),
162 corresponding to N-terminal methionine formylation (fMet), a well-known post-translational
163 modification occurring in bacterial protein synthesis¹⁸. From LC-UV data, it could be deduced that the
164 ratio of oxidized/reduced anti-HER2VHH is 32/68. These results highlight that the expression of anti-
165 HER2 VHH is more heterogeneous (C-terminal truncation and formylation) in *E. coli* than in *P.*
166 *pastoris*, the more homogeneous sample originating from synthetic chemistry with 100% of S-S
167 bridge formed.

168 *Native ion mobility-mass spectrometry of anti-HER2 VHH batches.* To gain insight into the VHH
169 construct conformations, we next used native MS hyphenated to ion mobility spectroscopy (IM-MS),
170 an emergent MS-based technique to assess protein conformational heterogeneities /homogeneities¹⁹⁻²².

171 Of note, no LC separation of VHH oxidized and reduced form is used upstream from the mass
172 spectrometer, leading to overlapping charge state distributions of both species in native MS (see
173 **Figure 5**); in these conditions, only the main form of the S-S bridge was observable. As expected, no
174 significant difference was observed on charge state distributions obtained in native conditions for the
175 different VHH constructs (**Figure 5**). We then turned on ion mobility (IM) and compared arrival time
176 distributions (ATDs) of VHH constructs (**Figure 6**). For the chemical synthetic VHH sample, a very
177 homogeneous Gaussian peak is detected for the 7⁺ charge state, with a FWHM of 1.3 ms. Interestingly,
178 increased ATD peak broadening is observed for *P. pastoris* (FWHM = 1.7 ms) and *E. coli* (FWHM =
179 2.0 ms) samples. Altogether, IM-MS results suggest very close conformational properties for the three
180 batches. However, as observed in LC-MS, the synthetic VHH seems to be more homogeneous in
181 terms of conformations, with thinner ATD peaks than the other constructs, in agreement with synthetic
182 VHH containing only S-S forms whereas the two other samples are mixtures of oxidized and reduced
183 VHH forms.

184 *Gas-phase conformational stability of anti-HER2 VHH batches by collision induced unfolding*
185 *experiments*. Finally, collision induced unfolding (CIU) experiments (**Figure 7**) were performed to
186 compare the gas-phase unfolding behavior of the three VHHs. This new approach has already been
187 reported for the rapid characterization of intact monoclonal antibodies²³⁻²⁶, fragments²⁷ and antibody
188 drug conjugates^{28,29}. Briefly, in CIU experiments, ions are progressively accelerated in the trap T-wave
189 of the mass spectrometer before IM separation in the IM cell. Drift times of the ions are reported as a
190 function of collision energies. The highly homogeneous chemical synthesis sample, containing only
191 the S-S form, presents a single conformational species ($t_D = 7.2$ ms) across the 0-120 V collision
192 energy range (**Figure 7**), suggesting a very stable construct resistant to gas phase unfolding across the
193 collision energy range. Conversely, the two others VHHs, containing a mixture of oxidized and
194 reduced forms, present a transition to a supplementary conformation in CIU experiments (See **Figure**
195 **7d**). This additional more extended conformation is observed at $t_D = 9.0$ ms from 30 to 120 V for
196 VHHs from *P. pastoris* and *E. coli*. The proportion of this second conformation is more abundant in
197 the *E. coli* VHH (39%) compare to the *P. pastoris* one (17 %). By converting t_D into averaged
198 collisional cross sections (CCS) of *E. coli* VHH, a variation from 13.2 nm² for the S-S form to 14.9
199 nm² for the reduced form is observed, resulting in a total increasing of 11.4 % in CCS between SS
200 initial state and the reduced form (**Table 3**).

201 This different gas phase unfolding behavior can be attributed to the presence of reduced VHH forms in
202 both samples. To unambiguously attribute the more extended conformation to the reduced form, we
203 compared the CIU fingerprint of the fully reduced VHH from *P. pastoris* to the original mixture
204 (**Figure 8**) and, as expected, we observed a stronger intensity of the extended conformation.
205 Interestingly, the ratios of oxidized and reduced forms coming either from IM-MS or LC-MS were
206 following the same trend. This difference in absolute values between IM-MS and LC-MS could be

207 explained by an insufficient resolution of the IM separation in CIU experiment for liable relative
208 quantification but enough for the detection of a second conformation more extended in this case.

209 Altogether, CIU results reflect higher heterogeneity of *P. pastoris* and *E. coli* samples compared to the
210 synthetic VHH. Oxidized and reduced VHH forms present different CIU behavior, suggesting a
211 specific CIU signature for both forms. CIU results highlight that disulfide bridge formation could be
212 characterized on a VHH and that it seems to stabilize, in our case, the anti-HER2 VHH structure.
213 Taken together, mass-spectrometry-based results have shown that *E. coli* does not permit the
214 expression of homogeneous VHH batch (formylation, truncation) nor a total formation of the disulfide
215 bridges. *P. pastoris* allows obtaining more homogeneous VHH batches while synthetic VHH is the
216 most homogenous form, with disulfide bridge being quantitatively formed.

217

218 **Functional characterization of VHH interaction with HER2 protein using surface plasmon** 219 **resonance (SPR)**

220 The binding capacity of VHH samples to the immobilized C-terminal part of HER2 protein was
221 assessed using SPR experiments. We first determined the active concentration of each VHH batch, by
222 measuring its ability to bind HER2 epitope, as it is not necessarily identical to the total concentration
223 reflected by the absorbance of the sample at 280 nm. Furthermore, a correct VHH concentration is
224 essential to determine affinity and the kinetic association rate constant. The percentage of active VHH
225 was determined by Calibration-Free Concentration Analysis (**Figure 9A to C**); it exceeded 80 % of
226 the soluble fraction for the three VHH sources (**Table 4**).

227 To measure the binding parameters of VHH samples, a low level of HER2 protein was immobilized
228 (100 RU) on a sensor surface. The binding rate was not affected by the flow rate (data not shown)
229 indicating that mass transport did not limit the interaction which is suitable for kinetic measurements.
230 The sensorgrams are presented in **Figure 9D to G**. As reported in **Table 5**, each anti-HER2 VHH
231 batch presents similar binding kinetics towards its antigen, which leads to comparable binding affinity
232 and kinetic constants regardless of the expression system.

233

234 Discussion

235 A boom in the area of antibody drug conjugates happened these last years with more than 300 clinical
236 trials. Furthermore, the possible use of smaller protein(s), with similar specificity than antibodies is
237 certainly a way to render this area more reachable to industrial scales. Indeed, a series of such
238 compounds are entering clinical trials and market. Thus, a growing interest occurred these last years
239 towards simplified antibodies, namely VHHs or nanobodies that comprise only a hundred amino acids.
240 Due to recent progress in the domain of peptide and protein synthesis (see review by Kent¹⁴), a
241 realistic option arises for the chemical synthesis of such small proteins. To us, it is clearly a great
242 advantage to move from recombinant to chemically-synthesized objects, and this for at least two
243 reasons: 1/ the industrial scalability of such compounds, intimately associated with the possibility to
244 achieve modern analytical characterization and 2/, more importantly, the possibility to include at *ad*
245 *hoc* places exotic amino acids, the side chain of which could bear a chemical function unique to a
246 given chemistry step, as opposed to cysteine- or lysine-based chemistry. Indeed, our recent work on
247 either ubiquitin¹² or an enzyme (calstabin, an isomerase)¹³ that were both chemically synthesized and
248 biologically active, as many other reported proteins (see Bacchi et al¹³ for listed examples and Kent¹⁴
249 for review) opens avenues on the possibility to access to proteins of small molecular weight (between
250 100 and 150 amino acids) and possibly to incorporate new exotic amino acids susceptible with
251 alternative, specific chemistry^{30,31}. This will provide new possibility of arming antibody-like proteins
252 such as VHHs, with cytotoxic compounds, potentially delivered to the right target-bearing cells. The
253 first steps to take, though, are the systematic study of such molecules, to characterize their folding and
254 their “antigen” recognition.

255 In order to be able to embark in such a task, the first step consisted to express various model VHHs in
256 various hosts, and to document thoroughly their characteristics, particularly regarding their structural
257 features . In parallel, we expressed the anti-HER2 VHH in two hosts and we synthesized the same
258 VHH for comparison purposes. Again, their respective biophysical characteristics were studied as well
259 as their capacity to recognize the antigen, HER2. The positive results we obtained paved the way
260 towards the possibility to synthesize VHHs in general while keeping their capacity to act as small
261 antibodies. Indeed, we did not record any major differences between the recombinant and the synthetic
262 protein. The main results in this stage 2 process were certainly the facts 1/ that a decent amount of
263 chemical VHH was obtained at a high purity level even if not at an industrial-compatible quantity, and
264 2/ that this product was not distinguishable from the recombinant one, despite a thorough
265 characterization, as we suggested as a result of the stage 1 process .

266 Gaining access to such a synthetic protein is of major importance, because it opens new avenues
267 according to two main axes: 1/ the possibility to modify the primary sequence of the VHH without
268 altering its affinity for its ‘antigen’ and 2/ the possibility to integrate almost any amino acid bearing an
269 alternative chemical function. The latter can, thanks to additional chemical steps, lead to VHH armed
270 with cytotoxic compounds, while maintaining their specificity towards therapeutic targets, chosen

271 because they are preferentially expressed in cancer cells, for example. Overall, those new compounds
272 will basically retain the specificity of their corresponding antibodies with an incredible gain in size, as
273 we would have proteins of ~140 aminoacids instead of the initial ~ 900 to ~ 1300 aminoacids
274 respectively composing camelid and other mammals antibodies. Not only the gain in absolute mass is
275 considerable, but also the structure of the VHH is far simpler than antibody's. Before embarking
276 further in such studies, as suggested below, the first step will be to rationalize the yield of such
277 synthesis. Indeed, it is only once the proof of concept has been done as in the present work that we
278 will be able to work out the various steps of the synthetic schemes, in order to render the process
279 scalable to a more industrial-friendly approach.

280 The stage 3 will consist of modifying this anti-HER2 VHH sequence with exotic amino acids at
281 position without negative influence on the HER2 recognition. In doing so, we will be able to introduce
282 chemical functions, orthogonal of cysteine and lysine side chain ones, leading to the possibility to
283 maintain a high specificity of the cargo – the VHH – while maintaining a cost-effective production, as
284 opposed to the monoclonal antibody option.

285

286

287 Material and Methods

288

289

290 Cloning, expression and purification of the anti-HER2 VHH in *E. coli*

291 In brief, the coding DNA fragment for the anti-HER2 VHH has been *E.coli* codon optimized,
292 synthesized and cloned into high copy expression vector with a poly-His-tag at the C-terminus end.
293 The genetic construct was transformed into the *E.coli* strain *Shuffle T7 express*. Bacteria were cultured
294 in a LB medium with ampicillin (final concentration of 100 µg/mL) and the expression was induced
295 when the OD at 600 nm reached 0.6 with 0.1 mM IPTG. The temperature was decreased from 37°C to
296 22°C for the expression and the expression time was over night. Cells were firstly harvested by
297 centrifugation (5000 g, 20 min, 4°C), and then lysed by lysozyme membrane digestion (1 mg/mL) into
298 a 20 mM Tris-HCl pH 8, 300 mM NaCl buffer supplemented with 10 µg/mL DNase1 and protease
299 inhibitor cocktail during 30 min at room temperature. Cell fragments were harvested by
300 ultracentrifugation (100000 x g, 30 min, 4°C). The supernatant was purified in three steps. A first step
301 using affinity properties of the His-tag for the Ni-NTA agarose resin (Qiagen) was performed. The
302 supernatant was injected onto an equilibrated Ni-NTA agarose resin with a 20 mM Tris-HCl pH 8,
303 300 mM NaCl, 10 mM imidazole buffer. The column was washed with the equilibrium buffer
304 supplemented with 20 mM imidazole, then the proteins were eluted with the equilibrium buffer
305 supplemented with 250 mM imidazole. The second purification step was performed by cation
306 exchange chromatography (IEX, SourceS, GE healthcare) after dialysis of the sample against a buffer
307 composed of 50 mM Tris-HCl pH 7.5, 50 mM NaCl. The sample was injected onto the cation
308 exchange column beforehand equilibrated with the dialysis buffer previously used. The proteins were
309 eluted using a gradient of a buffer composed of 50 mM Tris-HCl pH 7.5 and 1 M NaCl. The eluted
310 proteins were then concentrated by centrifugation using an Amicon (Millipore) with a cutoff of 3 kDa.
311 The concentrated sample was finally purified by sized exclusion chromatography (SEC) using a
312 HiLoad 26/600 Superdex 200 column (GE Healthcare) equilibrated with a 50 mM Tris-HCl pH 7.5,
313 150 mM NaCl buffer.

314 Cloning, expression and purification of the anti-HER2 VHH in *P. pastoris*

315 Anti-HER2 VHH DNA sequence was fused in frame to the α -factor secretion signal from
316 *Saccharomyces cerevisiae* on its 5' side and to a 6-His affinity tag sequence on its 3' side. It was
317 cloned in a modified expression vector from the pPIC9K series. The protease-deficient *P. pastoris*
318 strain SMD1163 was transformed with the linearized plasmid, and recombinant clones presenting a
319 stable VHH expression were selected based on both antibiotic resistance and expression level criteria,
320 as extensively described in Hartmann *et al.*³². For protein expression, cells were grown overnight in
321 BMGY (10 g/L yeast extract, 10 g/L peptone, 13.4 g/L yeast nitrogen base, 1 % (v/v) glycerol, 0.4
322 mg/L biotin, 100 mM potassium phosphate pH 6.0). On the next day, the cells were diluted in BMGY

323 and grown to an OD₆₀₀ of 5. The culture was centrifuged and the pellet resuspended in the same
324 volume of BMMY (10 g/L yeast extract; 10 g/L peptone, 13.4 g/L yeast nitrogen base, 0.5 % (v/v)
325 methanol, 0.4 mg/L biotin, 100 mM potassium phosphate pH 6.0) for induction of protein expression.
326 After 18 h at 22°C, the cells were spun down and the VHH-containing supernatant was either used
327 immediately for purification or frozen at -80°C. VHH-containing supernatant was incubated overnight
328 at 4°C with Ni-NTA agarose batch resin (Qiagen) previously equilibrated with purification buffer (25
329 mM Tris HCl at pH 7.4, 200 mM NaCl, 10 mM imidazole), at a ratio of 4 mL resin for 100 mL
330 supernatant. The resin was then poured into a disposable column and sequentially washed with (i)
331 purification buffer containing 25 mM imidazole, (ii) buffer containing 50 mM Tris HCl at pH 7.4, 1 M
332 NaCl. Purified VHH was then eluted with 5 mL elution buffer (25 mM Tris HCl at pH 7.4, 200 mM
333 NaCl, 250 mM imidazole). Imidazole was removed from the eluted fraction through dialysis in 50 mM
334 Tris HCl at pH 7.4, 150 mM NaCl. The final sample was concentrated using Vivaspin® Centrifugal
335 filter (membrane cut-off of 3 kDa) (VivaProducts, Gottigen, Germany). Except for the initial resin
336 incubation, all purification steps were performed at room temperature.

337

338 ***Chemical synthesis of anti-HER2 VHH***

339 A schematic representation of the synthesis strategy is shown in **Figure 2**. All peptides were
340 synthesized at 100 μmole scale using Fmoc-SPPS on a Symphony X instrument (Protein
341 Technologies, Inc., USA). Synthesis-grade Fmoc-AA reagents were purchased from Iris Biotech.
342 Specific L-pseudoproline dipeptides and (Dmb)Gly that were used to facilitate the peptide syntheses
343 are indicated in the peptide sequences in bold and underline font, respectively. HATU and 2-
344 chlorotriyl chloride resin (200-400 mesh, 1.2 mmol/g) were purchased from IRIS Biotech. DMF,
345 DCM, methanol, diethyl ether, and HPLC-grade acetonitrile were from purchased from Aldrich. The
346 standard deprotection-coupling cycle for each residue consisted of six steps: 1. Wash with 5 mL of
347 DMF (3 x 30 sec); 2. Deprotect Fmoc group with 5 mL of 20% piperidine in DMF (3 x 3 min); 3.
348 Wash with 5 mL of DMF (3 x 30 sec); 4. Couple Fmoc-AA (2 x 60 min); 4a. 5 mL of Fmoc-AA
349 dissolved at 200 mM in DMF; 4b. 2 mL of HATU dissolved at 500 mM in NMP; 4c. 2 mL of *i*Pr₂NEt
350 dissolved at 1 M in NMP; 5. Capping with 5 mL of 10% Ac₂O in DMF (7 min) and finally 6. Wash
351 with 5 mL of DMF (3 x 30 sec). Upon completion of the synthesis, peptide resins were washed 3 times
352 with DMF and 3 times with DCM. Peptide resins were then cleaved with one of three TFA cleavage
353 cocktails (per 100 μmole scale synthesis): a/ Cocktail #1 for peptides containing neither Met nor Cys:
354 18 mL TFA, 500 μL TIS, 500 mg Phenol, 1000 μL water; b/ Cocktail #2 for peptides containing Cys,
355 but not Met: 17.5 mL TFA, 500 μL TIS, 500 mg Phenol, 1000 μL water, 500 μL EDT; or c/ Cocktail
356 #3 for peptides containing Met: 17.5 mL TFA, 500 μL TIS, 500 mg Phenol, 1000 μL water, 500 μL
357 EDT and 500 μL tetrabutylammonium bromide. After 3 h of TFA cleavage, the cleavage solution was
358 filtered from the resin, and peptides were precipitated by addition to 40 mL of ice-cold ether. After >1
359 h at -20 °C, ether solutions were centrifuged at 3500 RCF, and the supernatants were decanted. Pellets

360 were washed twice more with ether, and then dried for >3 h in vacuum desiccator prior to dissolution,
361 analytical characterization, and purification. Peptides containing C-terminal acids and hydrazides were
362 used in this work. Peptide acids and hydrazides were custom loaded at low density (~0.2 mmol/g)
363 starting with 2-chlorotrityl chloride resin (1.5 mmol/g, IRIS Biotech, Germany). In the case of peptide
364 acids, 0.35 mmol Fmoc-AA was dissolved in 30 mL DCM, and then 1.5 mmol DIPEA was added to
365 the Fmoc-AA solution. This solution was next added to 1 g of resin and mixed for 2 h at room
366 temperature. Unreacted groups were capped with 17:2:1 DCM:MeOH:DIPEA for 30 min. Fmoc-AA-
367 resin was then washed 3x with DMF, 3x with DCM and vacuum dried for >20 min. The loading was
368 determined by the titration of the Fmoc group deprotection (UV, 301 nm). In the case of peptide
369 hydrazides, 0.35 mmol Fmoc-NH-NH₂ was dissolved in 30 mL DCM, and then 1.5 mmol DIPEA was
370 added to the solution. This solution was next added to 1 g of resin and mixed for 2 h at room
371 temperature. Unreacted groups were capped with 17:2:1 DCM:MeOH:DIPEA for 30 min. Fmoc-AA-
372 resin was then washed 3x with DMF, 3x with DCM and vacuum dried for >20 min. The loading was
373 determined by the titration of the Fmoc group deprotection (UV, 301 nm). Native chemical ligation
374 (NCL) reactions were performed according to standard methods using MPAA as thiol catalyst and
375 TCEP as reducing agent. Specifically, all ligation reactions employed peptide hydrazide method,
376 whereby peptides were dissolved and activated (conversion of hydrazide to acyl azide) in “activation
377 buffer” (6 M GuHCl, 100 mM phosphate, pH 3) for 20 min at -20 C by addition of freshly prepared 20
378 mM sodium nitrite. Following activation, a solution containing freshly prepared 200 mM MPAA pH 7
379 in “ligation buffer” (6 M GuHCl, 200 mM phosphate, pH 7) was added, and the final pH was adjusted
380 to 6.0-6.5 to initiate thiolysis and ligation reaction. Upon completion (based on analytical HPLC and
381 LC/MS), reactions were treated with freshly prepared 200 mM TCEP in 6 M GuHCl (pH > 6) for 10
382 min, spun at 5000 RCF to remove any aggregates, and the supernatant was purified by
383 preparative/semipreparative HPLC. The peptides were analyzed by UPLC and ESI-MS mass
384 spectrometry. The instruments were equipped with Jupiter 4 μm C12 Proteo 90 Å (250 x 21.2 mm)
385 (flow rate: 20 mL/min) or XBridge Protein BEH C4 4 μm 300 Å (250 x 19 mm) (flow rate: 20
386 mL/min). Solvents A and B were 0.1% TFA in H₂O and 0.1% TFA in MeCN, respectively.

387 *Synthesis of peptide F1*

388 The peptide F1 (EVQLVESGXGLVQAGGSLRLS-NHNH₂, see **Figure 3b**, blue peptide), where X is
389 G(H6-RMBO), was prepared by standard Fmoc-SPPS as described above, with a few special steps
390 elaborated below. The peptide chain was synthesized using standard Fmoc building blocks and
391 protecting groups, with the exception of the Fmoc-Gly(RMBO)-OH building block at the position
392 10. The N-terminus of the peptide was protected Boc-Glu(Otbu)-OH building block in cases. Upon
393 completion of the linear peptide synthesis, the alloc group was removed. PhSiH₃ (25 eq.) in 5 mL of
394 CH₂Cl₂ was added to the resin followed by Pd(PPh₃)₄ (0.25 eq.) in CH₂Cl₂. After agitating the resin for
395 1 h in the dark, the solution was drained and the reaction was repeated twice. The resin was washed

396 with 3 volumes of CH₂Cl₂, 4 volumes of 1M pyridine in DMF and 3 volumes of DMF. and standard
397 Fmoc-SPPS conditions were used to fuse the HisTag (His6) sequence to the VHH. Standard peptide
398 cleavage conditions (described above) were used following the synthesis of the HisTag with the
399 G(RMBO) part of the peptide. F1 crude peptide (350 mg) was dissolved in 20 mL of 25/75
400 acetonitrile/water (0.1% TFA) and purified on a Jupiter 4 μm C12 Proteo 90 Å (250 x 21.2 mm)
401 column using a gradient of 10 to 25% buffer B over 30 min. HPLC purification yielded 67 mg of pure
402 material. (yield 21%)

403 *Synthesis of peptide F2*

404 The peptide F2 (CAASGRTFSSYAMGWFRQAPGKEREFVVAINWSSGSTYYADSVKGRFTISRDN
405 NAKNTVYLQMNSLKPEDTAVYY-NH-NH₂, see **Figure 3b**, red peptide.) was prepared by
406 standard Fmoc-SPPS as described above, using standard Fmoc building blocks and protecting groups,
407 with the exception of the Fmoc-Asp(OEpe)-OH building block at the position 51, Fmoc-Asp(OtBu)-
408 Thr(psiMe,Mepro)-OH building block at the position 69 and , Fmoc-Asp(OtBu)-Ser(psiMe,Mepro)-
409 OH building block at the position 41. After standard peptide cleavage conditions (described above),
410 F2 crude peptide (900 mg) was dissolved in 20 mL of 25/75 acetonitrile/water (0.1% TFA) and
411 purified on a XBridge Protein BEH C4 4 μm 300 Å (250 x 19 mm) column using a gradient of 20 to
412 35% buffer B over 30 min. HPLC purification yielded 40 mg of pure material (yield 5%).

413

414 *Synthesis of peptide F3*

415 The peptide F3 (CNARWVKPQFIDNNYWGQGTQVTVSSHHHHHHH-OH, **Figure 3b**, green
416 peptide) was prepared by standard Fmoc-SPPS as described above, using standard Fmoc building
417 blocks and protecting groups. After standard peptide cleavage conditions (described above), the F3
418 crude peptide (650 mg) was dissolved in 20 mL of 25/75 acetonitrile/water (0.1% TFA) and purified
419 on a Jupiter 4 μm C12 Proteo 90 Å (250 x 21.2 mm) column using a gradient of 20 to 35% buffer B
420 over 30 min. HPLC purification yielded 80 mg of pure material. (yield 21%)

421

422 *Synthesis of peptide F1-2*

423 Native chemical ligation of F1 to F2 to generate F1-2 [EVQLVESGXGLVQAGG
424 SLRLSCAASGRTFSSYAMGWFRQAPGKEREFVVAINWSSGSTYYADSVKGRFTISRDN
425 VYLQMNSLKPEDTAVYY-NHNH₂ where X is G(H6-RMBO, **Figure 3c**, purple peptide)], was
426 performed using peptide hydrazide method. Here, 30 mg of F1 was dissolved in 3 mL of activation
427 buffer, and 40 mg of F2 was dissolved in 3 mL of ligation buffer. F1 was then activated (conversion of
428 hydrazide into azide) for 20 min at -20 °C by addition of 200 μL of 200 mM NaNO₂, pH 3.0. At the
429 same time, 100 mg of MPAA (200 mM) was dissolved in the F2 solution and the pH was adjusted to
430 6.5. After activation, the two solutions were mixed, and the final pH was adjusted to 6.5 to initiate
431 ligation. Reaction was complete after 6 h. The reaction was then reduced for 10 min by treatment with
432 100 mM TCEP at pH 7.5, then diluted out to 3 M GuHCl and washed with 4 x 5 mL of Et₂O. The

433 solution was adsorbed on affinity chromatography column (HiTrap™ Chelating HP, 5 mL) and the
434 column was washed with 3 x 5 mL of binding buffer (6 M GuHCl, 20 mM Na₂HPO₄, pH 7.5). The
435 product was eluted with 3 x 10 mL of elution buffer (6 M GuHCl, 20 mM Na₂HPO₄, 0.5 M Imidazole,
436 pH 7.5). The fractions containing the desired product were purified by HPLC on a XBridge Protein
437 BEH C4 4 μm 300 Å (250 x 19 mm) column using gradient of 20 – 45% B over 50 min. HPLC
438 purification yielded ~24 mg (45% yield, based on limiting F2 peptide) of pure material.

439

440 *Native chemical ligation between peptides F1-2 and F3.*

441 Native chemical ligation of F1-2 to F3 to generate F1-3
442 [EVQLVESGXGLVQAGGSLRLSCAASGRTFSSYAMGWFRQAPGKEREFVVAINWSSGSTYYA
443 DSVKGRFTISRDNKNTVYLQMNSLKPEDTAVYYCNARWVKPQFIDNNYWGQGTQVTVSS
444 HHHHHH-OH where X is G(H6-RMBO), **Figure 3c**, orange peptide)], was performed using the
445 peptide hydrazide method. Here, 24 mg of F1-2 was dissolved in 2 mL of activation buffer, and 17 mg
446 of F3 was dissolved in 2 mL of ligation buffer. F1-2 was then activated (conversion of hydrazide into
447 azide) for 20 min at -20 °C by addition of 200 μL of 200 mM NaNO₂, pH 3.0. At the same time, 65
448 mg of MPAA (200 mM) was dissolved in the F3 solution and the pH was adjusted to 6.5. After
449 activation, the two solutions were mixed, and the final pH was adjusted to 6.5 to initiate ligation.
450 Reaction was complete after 16 h. The reaction was then reduced for 10 min by treatment with 100
451 mM TCEP at pH 6.5, then diluted out to 3 M GuHCl and washed with 4 x 5 mL of Et₂O. The solution
452 was purified by HPLC on on a XBridge Protein BEH C4 4 μm 300 Å (250 x 19 mm) column using
453 gradient of 20 – 45% B over 50 min. HPLC purification yielded ~14 mg (45% yield, based on limiting
454 F2 peptide) of pure material.

455

456 *Synthesis of the anti-HER2 VHH*

457 The final anti-HER2 VHH (EVQLVESGGGLVQAGGSLRLSCAASGRTFSSYAMG
458 WFRQAPGKEREFVVINSSGSTYYADSVGRFTISRDNKNTVYLQMNSLKPEDTAVYYCNAR
459 WVKPQFIDNNYWGQGTQVTVSSHHHHHH-OH, **Figure 3c**, black peptide) was obtained by
460 dissolving 14 mg of the peptide F1-3-HisTag in 5 mL of TFA/DTT/iPr₃SiH (92.5:5:2.5) at room
461 temperature. After 5h, the peptide was precipitated with Et₂O, washed two times with Et₂O and
462 dissolved in 10 mL of 6M GuHCl solution. The solution was adsorbed on affinity chromatography
463 column (HiTrap™ Chelating HP, 5 mL) and the column was washed with 3 x 5 mL of binding buffer
464 (6 M GuHCl, 20 mM Na₂HPO₄, pH 7.5). The product was eluted with 3 x 5 mL of elution buffer (6 M
465 GuHCl, 20 mM Na₂HPO₄, 0.5 M Imidazole, pH 7.5). The peptide was desalting by solid phase
466 extraction using Sep-Pak C18 Cartridge (Waters, 2 g) and lyophilized yielding ~7 mg (53% yield) of
467 material.

468 *Folding of the synthetic VHH*

469 The peptide (7 mg) was dissolved in 50 mL of folding buffer (6 M GuHCl, 100 mM TRIS, pH 8.5)
470 and left 2 days at 4°C. The solution was purified by HPLC on a Jupiter 5 µm C4 300 Å (250x4.6 mm)
471 column using gradient of 20 – 40% B over 40 min at 70°C. HPLC purification yielded ~3.5 mg (50%
472 yield) of pure material. The solution containing peptide were lyophilised on a CHRIST Gamma 2-16
473 LSCplus for 24h at room temperature and 0.3 mbar.

474 ***SDS-PAGE electrophoresis***

475 Protein preparations were submitted to electrophoresis as follows. They were diluted twice in sample
476 buffer (100 mM Tris HCl at pH 6.8, 25 % glycerol, 8 % SDS, 0.2 g/L Coomassie Brilliant Blue G250,
477 200 mM DTT) and loaded on a 10 % polyacrylamide-SDS tricine gel, in parallel with PageRuler™
478 Prestained Protein Ladder (Thermo Scientific™). The separating layer of the gel was composed of 10
479 % acrylamide 19:1, 1 M Tris HCl at pH 8.45, 0.1 % SDS, 0.1 % (w/v) APS, 0.06 % (v/v) TEMED.
480 The stacking part was composed of 6 % acrylamide 19:1, 0.8 M Tris HCl at pH 8.45, 0.08 % SDS,
481 0.15 % (w/v) APS, 0.01 % (v/v) TEMED. Proteins were resolved for 1h at 100 V in tris-tricine buffer
482 (100 mM Tris HCl at pH 8.3, 100 mM tricine, 0.1 % SDS) and stained with Coomassie blue
483 (QuickCoomassie Stain, Generon, Slough, UK).

484

485 ***Dot-Blot***

486 Dot-blot assay was performed in a 96-well plate format using a Bio-dot microfiltration manifold
487 (Biorad). 25 µL of culture supernatant total was suspended in 25 µL sample buffer and absorbed onto
488 a 0.45-µm nitrocellulose membrane by gravity flow. The membrane was then washed three times with
489 200 µl of PBS per well. The immunodetection was performed using anti-His antibody (Penta-His
490 Antibody, Qiagen) diluted at 0.1 µg/mL in PBST containing 5 % (m/v) of BSA. Primary antibody
491 were revealed using secondary anti-mouse antibody coupled to a fluorophore (Goat anti-Mouse
492 antibody DyLight® 488 Conjugated, Bethyl Laboratories). The fluorescence signal was visualized on
493 an Odyssey scanner (Li-Cor).

494

495 ***Liquid chromatography coupled to mass spectrometry (LC-MS)***

496 Liquid chromatography coupled to mass spectrometry (LC-MS) analysis were performed using an
497 Alliance 2695 (Waters, MA USA) coupled to a micrOTOF-Q (Bruker, Billerica, MA, USA). A
498 volume equivalent to 15 µg of sample preparation was injected on a XBridge BEH300, C4, 3.5µm, 2.1
499 x 150 mm column (Waters) set at 60°C. The gradient was generated at a flow rate of 250 µL/min
500 using 0.1% trifluoroacetic acid (TFA) for mobile phase A and acetonitrile containing 0.08% TFA for
501 mobile phase B. B was raised from 20 to 60% in 20 min followed by a 2 min washing step at 90% B
502 and a 15 min reequilibration period. Signal acquisition was realized by UV absorbance measurement
503 at 214 nm. The micrOTOF-Q was operated in positive mode with a capillary voltage of 4500 V.
504 Acquisitions were performed on the mass range 500-5000 m/z with a 1 s scan time. External mass

505 calibration of the TOF was achieved before each set of analyses using Tuning Mix (Agilent
506 Technologies, Paolo Alto, USA) in the mass range of 622-2732 m/z. Data analysis was performed
507 using Compass DataAnalysis 4.2 software (Bruker).

508

509 ***Native mass spectrometry and ion mobility mass spectrometry (IM-MS)***

510 Prior to native MS and IM-MS experiments, all anti-HER2 VHHs were buffer exchanged against
511 ammonium acetate (150 mM, pH 7.4) buffer (Sigma, St. Louis, MO, USA), using Zeba Spin desalting
512 columns (Thermo Fisher Scientific, Rockford, IL, USA). Sample concentrations were determined by
513 UV absorbance using a NanoDrop 2000 spectrophotometer (Thermo Fisher Scientific). Native mass
514 spectrometry analysis were carried out on a hybrid electrospray quadrupole time-of-flight mass
515 spectrometer (Synapt G2 HDMS, Waters, Manchester, UK) coupled to an automated chip-based
516 nanoelectrospray source (Triversa Nanomate, Advion Biosciences, Ithaca, U.S.A.) operating in the
517 positive ion mode. Mass spectrometer calibration was performed using singly charged ions produced
518 by a 2 mg/ml solution of cesium iodide in 2-propanol/water (1v/1v) over the m/z range 500–8000.
519 Instrumental parameters have been optimized to get optimal high m/z ion transmission and resolution
520 by raising the backing pressure to 6 mbar and the cone voltage to 20 V. Data interpretation was
521 performed using MassLynx 4.1 (Waters, Manchester, UK). Ion mobility experiments were performed
522 on a TWIMS-MS Synapt G2 instrument (Waters, Manchester, UK). MS and IMS parameters were
523 carefully tuned in order to obtain good IM resolution without ion activation using low accelerating
524 voltages. In the Z-spray source, sampling cone was fixed to 20 V and the backing pressure to 6 mbar.
525 For IM-MS characterization, the IM cell parameters have been optimized as described below. The
526 argon flow rate in the traveling-wave based ion trap was 5 mL/min and the trap collision voltage has
527 been set to 4 V. In the helium compartment, ions were thermalized with a flow rate of 120 mL/min
528 and the ion mobility cell was filled with a constant N₂ flow rate of 30 mL/min for ion separation. The
529 IM wave height and velocity were set 30 V and 1000 m/s, respectively. After the IM cell, the transfer
530 collision voltage was fixed to 2 V in order to transmit ions up to the TOF analyzer. Ion mobility
531 calibration was performed using β -lactoglobulin as described elsewhere³³ in order to calculate
532 collision cross sections for each anti-HER2 VHH batch. IM-MS measurements were performed in
533 triplicate under identical conditions.

534

535 ***Collision induced unfolding experiments (CIU)***

536 We also characterized our proteins by collision-induced unfolding experiments. Ions were activated in
537 the trap cell by increasing progressively the trap collision voltage in 5 V steps from 0 to 120 V prior to
538 IM separation during 1 min run. Generation and data interpretation of CIU plots were performed using
539 the open-source CIU_Suite software, allowing the extraction of the arrival time distribution (ATD) of
540 ions of interest at each trap collision voltage as described previously^{27,22}.

541

VHH-“antigen” interaction measurements

SPR experiments were performed to measure the interactions between antibodies and HER2 protein were investigated using a BIAcore T200 at 25 °C. Sensor surfaces CM5 sensorchips (BR100530), amine coupling kit and other Biacore consumables were purchased from GE Healthcare. HER2 protein was immobilized on the sensor surface and the VHH antibodies were injected over the surface in a continuous flow. To immobilize HER2 protein onto the chips, we used standard amine coupling procedures³⁴ at a flow rate of 10 $\mu\text{L}/\text{min}$ in a running buffer composed of 10 mM HEPES at pH 7.4, 150 mM NaCl, 0.05 % P20 surfactant. Surfaces were activated by an injection of a 1:1 mix of 0.2 M N-ethyl- N'-(3-dimethylaminopropyl)-carbodiimide hydrochloride (EDC) and 0.05 M N-hydroxysuccinimide (NHS) for 10 min. The his-tagged N-terminal extracellular domain of human HER2 protein (Sino Biological, Cat. Number 10004-H08H) was diluted at a concentration of 5 and 25 $\mu\text{g}/\text{mL}$ in acidic sodium acetate buffer (pH 5.5) and injected on two chip surfaces, until immobilization reached the respective levels of 100 RU and 1200 RU. The remaining active groups were then deactivated with an injection of ethanolamine hydrochloride (1 M pH 8.5). Reference surfaces were treated similarly except that HER2 injection was omitted. VHH samples were prepared in 50 mM Tris HCl at pH 7.5, 400 mM NaCl and 0.05% P20 surfactant, which constitute the running buffer. All the samples and blanks were injected in duplicate. The HER2 surfaces were regenerated with two successive injections (10 s) of 3 M MgCl_2 . The concentration measurements, using Calibration-Free Concentration Analysis (CFCA), were performed as follows: the VHH samples (1 nM) were injected for 60 s on the high-density immobilized surface, at flow rates of 10 $\mu\text{L}/\text{min}$ and 80 $\mu\text{L}/\text{min}$. For each sample, the dilution was globally fitted using the CFCA functionality in Biacore T200 evaluation software v 1. For the analysis, a diffusion coefficient of $1.28 \times 10^{-10} \text{ m}^2/\text{s}$ and a VHH molecular weight of 14024 Da were used. Concentration measurements validation criteria were those recommended by Biacore, *i.e.* a sufficiently high initial binding rate at low flow (about 0.2 to 0.3 $\text{RU}\cdot\text{s}^{-1}$ at 5 $\mu\text{L}/\text{min}$) and limited by mass transport visible as binding curves spread out when binding rates are dependent of flow rate. The degree of mass transport limitation was estimated by the QC ratio which vary from 0 to 1 for kinetic or totally mass transport controlled interaction^{35,36}. The kinetic and affinity were measured as follows: VHH samples at concentrations in the 0.25 nM to 30 nM ranges were serially injected for 300 s over reference and HER2 surfaces. Each VHH injection was followed by a 900 s buffer. The flow rate was 50 $\mu\text{L}/\text{min}$. SPR data were processed using the softwares BIAevaluation T200 evaluation version 1 or Scrubber 2.0c (BioLogic Software, Campbell, Australia). Sensorgrams were automatically XY-zeroed before the injection start and corrected for signals recorded on the empty reference surface. The overlaid sensorgrams were further processed by subtracting the average of the three to five running buffer responses^{37,38}. The protein concentration was determined from the binding data on the high-density HER2 surface using the CFCA evaluation feature of the BIAevaluation T200 software. The association (k_{on}) and dissociation (k_{off}) rate constants,

578 the dissociation equilibrium constant ($K_D = k_{off}/k_{on}$), the maximum response R_{max} were determined
579 using a simple 1:1 Langmuir interaction model by regression analysis.

580

581

582

583

584

585

586 **Acknowledgements** This work was supported by the several sponsors (Région Alsace, Communauté
587 Urbaine de Strasbourg, CNRS, and the Université de Strasbourg), by the Agence Nationale de la
588 Recherche (ANR) and the French Proteomic Infrastructure (ProFI; ANR-10-INBS-08-03). We thank
589 GIS IBiSA and Région Alsace for financial support in purchasing a Synapt G2 HDMS instrument. T.
590 Botzanowski acknowledges Institut de Recherche Servier for funding of his PhD fellowship.

591

592

593 The authors declare no conflict of interest.

Table 1: Detailed protein sequences

Production source	Amino acid sequence	Size	Theoretical mass (Da)
<i>E. coli</i>	MEVQLVESGGGLVQAGGSLRLSCATSGITFMRY ALGWYRQSPGKQREMVASINSGGTTNYADSVK GRFTISRDNKNTVYLMNSLKPEDTAVYYCNA RWVKPQFIDNNYWGQGTQVTVSSHHHHHH*	127 AA	14155.8 Da
<i>P. pastoris</i>	<u>MRFPSIFTAVLFAASSALAAPVNTTTEDETAQIPA</u> <u>EAVIGYSDLEGDFDVAVLPFSNSTNGLLFINTTI</u> ASIAAKEEGVSLEKRGSEVQLVESGGGLVQAGG SLRLSCATSGITFMRYALGWYRQSPGKQREMV SINSGGTTNYADSVKGRFTISRDNKNTVYLM NSLKPEDTAVYYCNARWVKPQFIDNNYWGQGT QVTVSSHHHHHH*	128 AA	14168.7 Da
Chemical synthesis	EVQLVESGGGLVQAGGSLRLSCATSGITFMRYA LGWYRQSPGKQREMVASINSGGTTNYADSVKG RFTISRDNKNTVYLMNSLKPEDTAVYYCNAR WVKPQFIDNNYWGQGTQVTVSSHHHHHH*	126 AA	14024.6 Da

Underlined sequence: α -factor secretion signal from *Saccharomyces cerevisiae*. It is endogenously cleaved by the yeast KEX2 protease during protein maturation in the Golgi apparatus. Protein size and molecular weight are given without this secretion signal.

Table 2 : Identification of anti-HER2 VHH species by liquid chromatography coupled to mass spectrometry.

Anti-HER2 VHH batch	Peak annotation	Time (min)	Mass (Da)	Species
<i>Chemical synthesis</i>	I	15.1	14022.7 ± 0.3	S-S form
	I	13.5	14166.9 ± 0.5	S-S form
<i>P. pastoris</i>	II	14.9	14168.9 ± 0.4	SH form
	I	15.3	14153.9 ± 0.3	S-S form WT
<i>E. coli</i>	II	15.5	13605.4 ± 0.2	S-S form truncated
	III	16.6	14155.9 ± 0.5	SH form WT
	IV	16.8	13607.6 ± 0.4	SH form truncated
	V	17.4	14183.9 ± 0.2	SH form WT +fMet
	VI	17.5	13635.5 ± 0.4	SH form truncated + fMet

Table 3: Table summarizing all the experimental $^{TW}CCS_{N_2}$ measurements

<i>Z</i>	Trap CV= 4 V (initial state)			Trap CV= 35 V (extended conformation)		
	<i>Chemical synthesis</i>	<i>P. pastoris</i>	<i>E. coli</i>	<i>Chemical synthesis</i>	<i>P. pastoris</i>	<i>E. coli</i>
	$^{TW}CCS_{N_2}$ (nm ²)	$^{TW}CCS_{N_2}$ (nm ²)	$^{TW}CCS_{N_2}$ (nm ²)			
6	11.8 ± 0.1	11.9 ± 0.1	12.0 ± 0.1	-	-	-
7	13.0 ± 0.1	13.1 ± 0.1	13.2 ± 0.1	-	15.0 ± 0.1	14.9 ± 0.1
8	14.5 ± 0.1	14.5 ± 0.1	14.5 ± 0.1	-	-	-
-	14.2*	14.3*	14.3*	-	-	-

$^{TW}CCS_{N_2}$ measurements measured in native IM+MS conditions (trap CV=4V) are denoted with the standard deviation for each individual charge state (standard deviation has been calculated from three different analysis) and the theoretical $^{TW}CCS_{N_2}$ values calculated from $CCS = 2.435 \times (M)^{(2/3)}$ (asterisk)³⁹. $^{TW}CCS_{N_2}$ values ranging from 11.8 to 14.5 nm² were obtained for the 6⁺ from 8⁺ charge states. Measured $^{TW}CCS_{N_2}$ values of the 8⁺ charge state (14.5 nm²) were in good agreement with both predicted collision cross-section from VHHs considered as spherical proteins (14.2-14.3 nm²).

Table 4: Binding parameters of anti-HER2 VHH to its antigen HER2 determined by SPR (n=2)

Expression organism	k_{on} ($\text{M}^{-1} \cdot \text{s}^{-1}$)	k_{off} (s^{-1})	K_{D} (nM)	R_{max}
<i>E. coli</i>	$2.0\text{E}6 \pm 0.4\text{E}6$	$5.6\text{E}-3 \pm 0.2\text{E}-3$	2.8 ± 0.5	13.2 ± 1.1
<i>P. pastoris</i>	$2.1\text{E}6 \pm 0.3\text{E}6$	$4.4\text{E}-3 \pm 0.2\text{E}-3$	2.1 ± 0.4	13.2 ± 2.1
<i>Chemical synthesis</i>	$2.5\text{E}6 \pm 0.9\text{E}6$	$2.8\text{E}-3 \pm 0.4\text{E}-3$	1.3 ± 0.6	12.0 ± 1.7

Table 5: Percentage of active anti-HER2 VHH in each batch determined by SPR

Expression organism	Soluble fraction (%)	Total protein concentration (M)	Active protein concentration (M)	Ratio of active VHH (%)
<i>E. coli</i>	100 %	1.20E-04	1.02E-04	85 %
<i>P. pastoris</i>	100 %	1.90E-05	1.88E-05	99 %
<i>Chemical synthesis</i>	18 %	7.70E-06	7.39E-06	96 %

Legends to the figures:

Figure 1. SDS-PAGE analysis of anti-HER2 VHH batches. Migration of $\sim 2 \mu\text{g}$ purified anti-HER2 VHH in each lane. MW: Molecular Weight ladder. Pp: *Pichia pastoris* expression system. Ec: *Escherichia coli* expression system. Synth: chemical synthesis.

Figure 2. Schematic representation of the strategy for the chemical synthesis of anti-HER2 VHH. (a) Anti-HER2 VHH amino acid sequence. (b) Amino acid sequences of the various peptide segments; X indicates position of the linker RMBO incorporation at the Gly9 residue. (c) Synthetic strategy.

Figure 3. Analytical data for the characterization of the various peptides of the anti-HER2 VHH chemical synthesis. a) HPLC traces and deconvoluted MS for initial peptide segments F1 (blue), F2 (red), and F3 (green). (b) HPLC trace and deconvoluted MS of first purified ligation product F1-2. (c) HPLC trace and deconvoluted MS of purified ligation product F1-2-3 (d) HPLC trace and deconvoluted MS of final product full-length VHH anti-HER2

Figure 4. Heterogeneity/homogeneity assessment of anti-HER2 VHH batches by LC-UV-MS and native MS. HPLC-MS analysis in denaturing conditions of anti-HER2 VHH batches (left panel): *Chemical synthesis* batch (a), *P. pastoris* batch (b) and *E. coli* batch (c) UV chromatograms.

Figure 5. Native mass spectrometry analysis of anti-HER2 VHH batches. ESI mass spectra on the m/z range [1000-3500] of Chemical synthesis (a), *P. pastoris* (b) and *E. coli* (c) batches in native conditions obtained on a Q-TOF instrument. a) (A) $14\ 022.4 \pm 0.4 \text{ Da}$: VHH WT ($7+/2004.1 \text{ m/z}$) ; (*) $14\ 085.1 \pm 0.4 \text{ Da}$ (+63 Da) : VHH WT (+non covalent adduct). b) (B) $14\ 166.4 \pm 0.5 \text{ Da}$: VHH WT ($7+/2024.9$); (*) $14\ 229.2 \pm 0.4 \text{ Da}$ (+63 Da) : VHH WT (+non covalent adduct). c) (C) $14\ 155.1 \pm 0.4 \text{ Da}$: VHH WT ($7+/2023.1 \text{ m/z}$); (#) $14\ 183.2 \pm 0.5 \text{ Da}$ (+28 Da) : VHH WT (+fMet); (D) $13\ 607.7 \pm 0.5 \text{ Da}$: C-ter truncated VHH (1-123) ($7+/1944.7 \text{ m/z}$); (#) $13\ 635.7 \pm 0.5 \text{ Da}$ (+28 Da) : C-ter truncated VHH (+fMet). (*) and (#) represent a non-covalent adduct and a formylation, respectively.

Figure 6. Native IM-MS experiments for conformational characterization of anti-HER2 VHH batches. ATDs of the $7+$ charge state of the three VHHs at low collision energy (4V).

Figure 7. Gas-phase conformational stability of anti-HER2 VHH batches by Collision Induced Unfolding experiments. CIU plots of anti-HER2 VHH batches. CIU fingerprints of the $7+$ charge state for the VHH from *Chemical synthesis* (a), *P. pastoris* (b) and *E. coli* (c) batches from 0 to 120 V collision energies. ATD extraction of the $7+$ charge state of the three VHHs at 35 V collision energy (d).

Figure 8: Gas-phase conformational stability of non-reduced and reduced anti-HER2 VHH produced by *P. pastoris*. CIU plots of the $7+$ charge state for the non-reduced (a) and reduced (b) anti-HER2 VHH samples.

Figure 9: Functional characterization of VHH-antigen interaction by SPR. Panels A to C: Calibration-Free Concentration Analysis of VHH active concentration. CFCA fits for the binding between highly immobilized HER2 antigen (1200 RU) and a VHH dilution ($\sim 1 \text{ nM}$) tested in duplicates at two different flow rates (10 and $80 \mu\text{L}\cdot\text{min}^{-1}$). The VHH samples were prepared from (A) *E. coli* periplasmic expression (B) chemical synthesis (C) *P. pastoris* secretion. The figures show overlay plots of experimental (black) and calculated (red) data. Calculated concentration in nM, closeness of the fit (χ^2) and degree of mass transport limitation (QC ratio) for each sample: A: 0.85 nM, $\chi^2 = 0.022$, QC ratio = 0.691; B: 0.99 nM, $\chi^2 = 0.047$, QC ratio = 0.662; C 0.96 nM, $\chi^2 = 0.011$, QC ratio = 0.718. Panels D to G: Sensorgrams of the interaction between immobilized HER2

antigen (100 RU) and increasing concentrations of VHH (0.33, 1, 3.33, 10, 30 nM, duplicates). (D) *E. coli* periplasmic expression (E) chemical synthesis (F) *P. pastoris* secretion (G) anti-ADORA2A VHH, negative control. For D, E and G, experimental curves (black) were fitted with a 1:1 Langmuir binding model (red) using scrubber 2.0c software, residual plots obtained in global analysis of each binding curves are shown and are randomly distributed.

References

1. Bertoli, G, Cava, C, and Castiglioni, I (2015) MicroRNAs: New Biomarkers for Diagnosis, Prognosis, Therapy Prediction and Therapeutic Tools for Breast Cancer. *Theranostics* 5:1122–1143.
2. Godfrey, C, Desviat, LR, Smedsrød, B, Piétri-Rouxel, F, Denti, MA, Disterer, P, Lorain, S, Nogales-Gadea, G, Sardone, V, Anwar, R, El Andaloussi, S, Lehto, T, Khoo, B, Brolin, C, van Roon-Mom, WM, Goyenvalle, A, Aartsma-Rus, A, and Arechavala-Gomez, V (2017) Delivery is key: lessons learnt from developing splice-switching antisense therapies. *EMBO Mol Med* 9:545–557.
3. Singh, A, Trivedi, P, and Jain, NK (2018) Advances in siRNA delivery in cancer therapy. *Artif Cells Nanomed Biotechnol* 46:274–283.
4. Campbell, A, Brieva, T, Raviv, L, Rowley, J, Niss, K, Brandwein, H, Oh, S, and Karnieli, O (2015) Concise Review: Process Development Considerations for Cell Therapy. *Stem Cells Transl Med* 4:1155–1163.
5. Cahn, A, Miccoli, R, Dardano, A, and Del Prato, S (2015) New forms of insulin and insulin therapies for the treatment of type 2 diabetes. *The Lancet Diabetes & Endocrinology* 3:638–652.
6. Shepard, HM, Phillips, GL, D Thanos, C, and Feldmann, M (2017) Developments in therapy with monoclonal antibodies and related proteins. *Clin Med (Lond)* 17:220–232.
7. Acheampong, DO, Adokoh, CK, Ampomah, P, Agyirifor, DS, Dadzie, I, Ackah, FA, and Asiamah, EA (2017) Bispecific Antibodies (bsAbs): Promising Immunotherapeutic Agents for Cancer Therapy. *Protein Pept Lett* 24:456–465.
8. Goldman, ER, Liu, JL, Zabetakis, D, and Anderson, GP (2017) Enhancing Stability of Camelid and Shark Single Domain Antibodies: An Overview. *Front. Immunol.* 8:865.
9. Muyldermans, S (2013) Nanobodies. *Annu. Rev. Biochem.* 82:775–797.
10. van Bockstaele, F, Holz, J-B, and Revets, H (2009) The development of nanobodies for therapeutic applications. *Curr Opin Investig Drugs* 10:1212–1224.
11. Skerra, A (2007) Alternative non-antibody scaffolds for molecular recognition. *Curr Opin Biotechnol* 18:295–304.
12. Bacchi, M, Fould, B, Jullian, M, Kreiter, A, Maurras, A, Nosjean, O, Coursindel, T, Puget, K, Ferry, G, and Boutin, JA (2017) Screening ubiquitin specific protease activities using chemically synthesized ubiquitin and ubiquitinated peptides. *Anal Biochem* 519:57–70.
13. Bacchi, M, Jullian, M, Sirigu, S, Fould, B, Huet, T, Bruyand, L, Antoine, M, Vuillard, L, Ronga, L, Chavas, LMG, Nosjean, O, Ferry, G, Puget, K, and Boutin, JA (2016) Total chemical synthesis, refolding, and crystallographic structure of fully active immunophilin calstabin 2 (FKBP12.6). *Protein Sci* 25:2225–2242.
14. Kent, SBH (2019) Novel protein science enabled by total chemical synthesis. *Protein Sci* 28:313–328.
15. Zheng, J-S, Yu, M, Qi, Y-K, Tang, S, Shen, F, Wang, Z-P, Xiao, L, Zhang, L, Tian, C-L, and Liu, L (2014) Expedient total synthesis of small to medium-sized membrane proteins via Fmoc chemistry. *J Am Chem Soc* 136:3695–3704.

16. Loibl, SF, Harpaz, Z, Zitterbart, R, and Seitz, O (2016) Total chemical synthesis of proteins without HPLC purification. *Chem Sci* 7:6753–6759.
17. Fang, G-M, Li, Y-M, Shen, F, Huang, Y-C, Li, J-B, Lin, Y, Cui, H-K, and Liu, L (2011) Protein chemical synthesis by ligation of peptide hydrazides. *Angew Chem Int Ed Engl* 50:7645–7649.
18. Kozak, M (1983) Comparison of initiation of protein synthesis in procaryotes, eucaryotes, and organelles. *Microbiol Rev* 47:1–45.
19. Atmanene, C, Wagner-Rousset, E, Malissard, M, Chol, B, Robert, A, Corvaña, N, van Dorselaer, A, Beck, A, and Sanglier-Cianfèrani, S (2009) Extending Mass Spectrometry Contribution to Therapeutic Monoclonal Antibody Lead Optimization: Characterization of Immune Complexes Using Noncovalent ESI-MS. *Anal. Chem.* 81:6364–6373.
20. Shepherd, DA, Holmes, K, Rowlands, DJ, Stonehouse, NJ, and Ashcroft, AE (2013) Using Ion Mobility Spectrometry–Mass Spectrometry to Decipher the Conformational and Assembly Characteristics of the Hepatitis B Capsid Protein. *Biophysical Journal* 105:1258–1267.
21. Pritchard, C, O’Connor, G, and Ashcroft, AE (2013) The Role of Ion Mobility Spectrometry–Mass Spectrometry in the Analysis of Protein Reference Standards. *Anal. Chem.* 85:7205–7212.
22. Terral, G, Beck, A, and Cianfèrani, S (2016) Insights from native mass spectrometry and ion mobility-mass spectrometry for antibody and antibody-based product characterization. *J Chromatogr B Analyt Technol Biomed Life Sci* 1032:79–90.
23. Hernandez-Alba, O, Wagner-Rousset, E, Beck, A, and Cianfèrani, S (2018) Native Mass Spectrometry, Ion Mobility, and Collision-Induced Unfolding for Conformational Characterization of IgG4 Monoclonal Antibodies. *Anal. Chem.* 90:8865–8872.
24. Huang, Y, Salinas, ND, Chen, E, Tolia, NH, and Gross, ML (2017) Native Mass Spectrometry, Ion mobility, and Collision-Induced Unfolding Categorize Malaria Antigen/Antibody Binding. *J Am Soc Mass Spectrom* 28:2515–2518.
25. Tian, Y, Han, L, Buckner, AC, and Ruotolo, BT (2015) Collision Induced Unfolding of Intact Antibodies: Rapid Characterization of Disulfide Bonding Patterns, Glycosylation, and Structures. *Anal. Chem.* 87:11509–11515.
26. Pisupati, K, Tian, Y, Okbazghi, S, Benet, A, Ackermann, R, Ford, M, Saveliev, S, Hosfield, CM, Urh, M, Carlson, E, Becker, C, Tolbert, TJ, Schwendeman, SP, Ruotolo, BT, and Schwendeman, A (2017) A Multidimensional Analytical Comparison of Remicade and the Biosimilar Remsima. *Anal. Chem.* 89:4838–4846.
27. Tian, Y, and Ruotolo, BT (2018) Collision induced unfolding detects subtle differences in intact antibody glycoforms and associated fragments. *International Journal of Mass Spectrometry* 425:1–9.
28. Botzanowski, T, Erb, S, Hernandez-Alba, O, Etkirch, A, Colas, O, Wagner-Rousset, E, Rabuka, D, Beck, A, Drake, PM, and Cianfèrani, S (2017) Insights from native mass spectrometry approaches for top- and middle- level characterization of site-specific antibody-drug conjugates. *MAbs* 9:801–811.
29. Tian, Y, Lippens, JL, Netirojjanakul, C, Campuzano, IDG, and Ruotolo, BT (2019) Quantitative collision-induced unfolding differentiates model antibody-drug conjugates. *Protein Sci* 28:598–608.

30. Hinner, MJ, and Johnsson, K (2010) How to obtain labeled proteins and what to do with them. *Curr Opin Biotechnol* 21:766–776.
31. Sletten, EM, and Bertozzi, CR (2009) Bioorthogonal Chemistry: Fishing for Selectivity in a Sea of Functionality. *Angew. Chem. Int. Ed.* 48:6974–6998.
32. Hartmann, L, Kugler, V, and Wagner, R (2016) Expression of Eukaryotic Membrane Proteins in *Pichia pastoris*. *Methods Mol Biol* 1432:143–162.
33. Bush, MF, Hall, Z, Giles, K, Hoyes, J, Robinson, CV, and Ruotolo, BT (2010) Collision cross sections of proteins and their complexes: a calibration framework and database for gas-phase structural biology. *Anal. Chem.* 82:9557–9565.
34. Johnsson, B, Löfås, S, and Lindquist, G (1991) Immobilization of proteins to a carboxymethyl-dextran-modified gold surface for biospecific interaction analysis in surface plasmon resonance sensors. *Anal Biochem* 198:268–277.
35. Pol, E, Roos, H, Markey, F, Elwinger, F, Shaw, A, and Karlsson, R (2016) Evaluation of calibration-free concentration analysis provided by Biacore™ systems. *Anal Biochem* 510:88–97.
36. Karlsson, R (2016) Biosensor binding data and its applicability to the determination of active concentration. *Biophys Rev* 8:347–358.
37. Myszka, DG (1999) Improving biosensor analysis. *J. Mol. Recognit.* 12:279–284.
38. Myszka, DG, Wood, SJ, and Biere, AL (1999) [25] Analysis of fibril elongation using surface plasmon resonance biosensors, in *Amyloid, Prions, and Other Protein Aggregates*, pp 386–402, Elsevier
39. Ruotolo, BT, Benesch, JLP, Sandercock, AM, Hyung, S-J, and Robinson, CV (2008) Ion mobility-mass spectrometry analysis of large protein complexes. *Nat Protoc* 3:1139–1152.

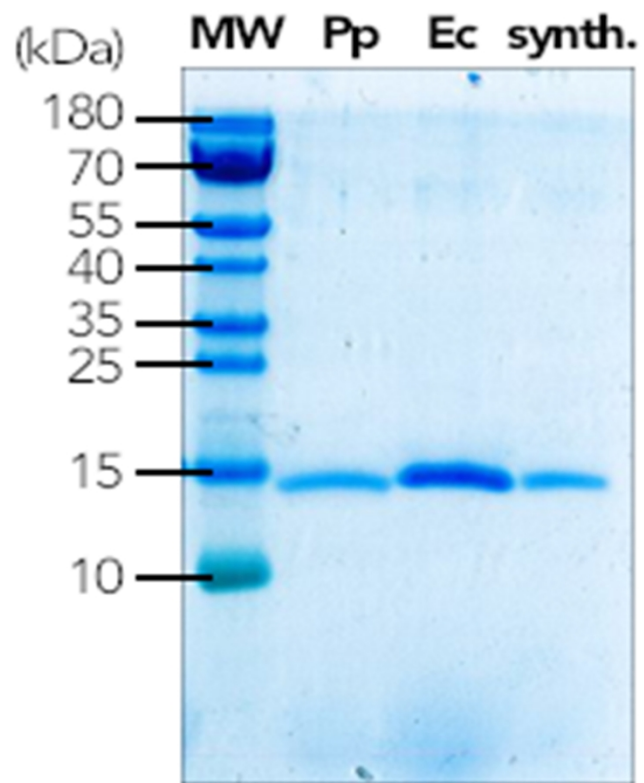


Figure 1

Figure 1

190x254mm (300 x 300 DPI)

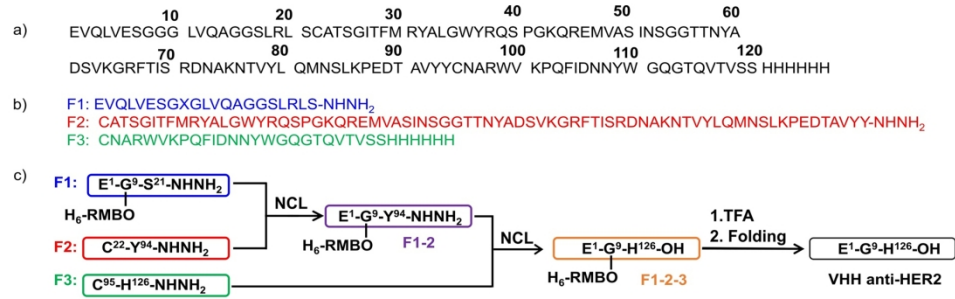


Figure 2

Figure 2

254x190mm (300 x 300 DPI)

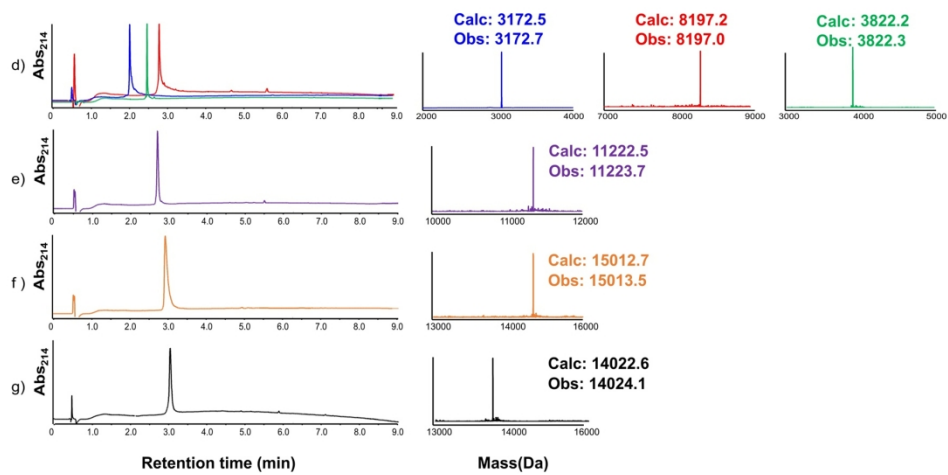


Figure 3

Figure 3

254x190mm (300 x 300 DPI)

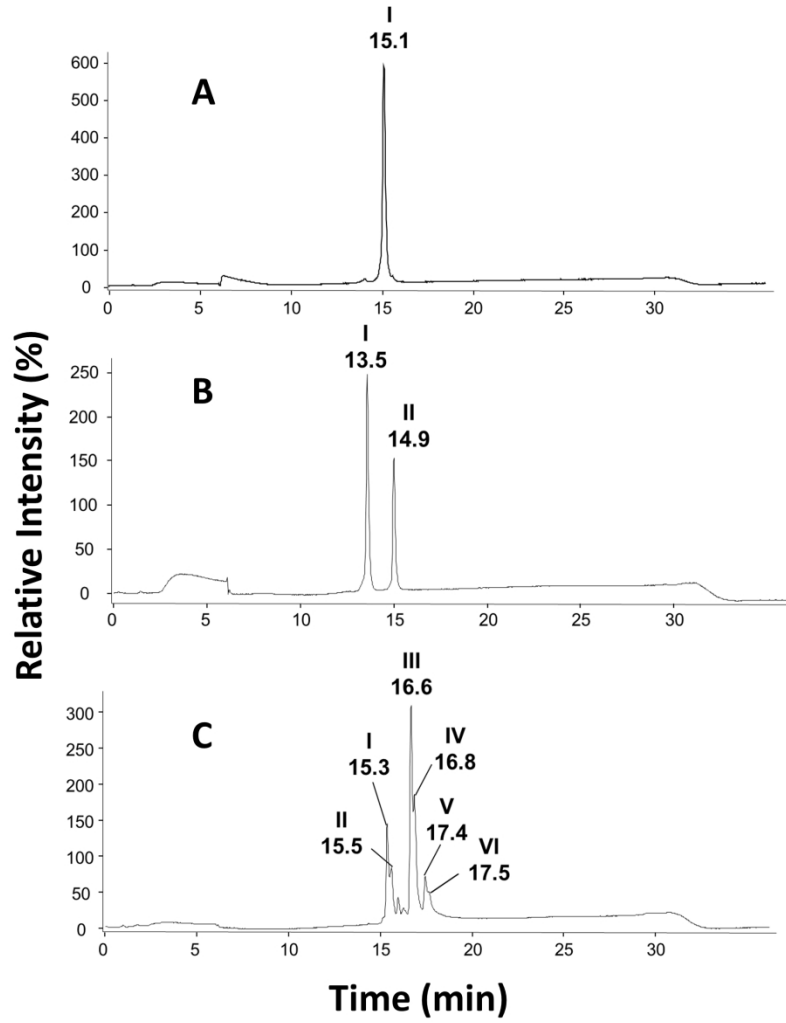


Figure 4

Figure 4

190x254mm (300 x 300 DPI)

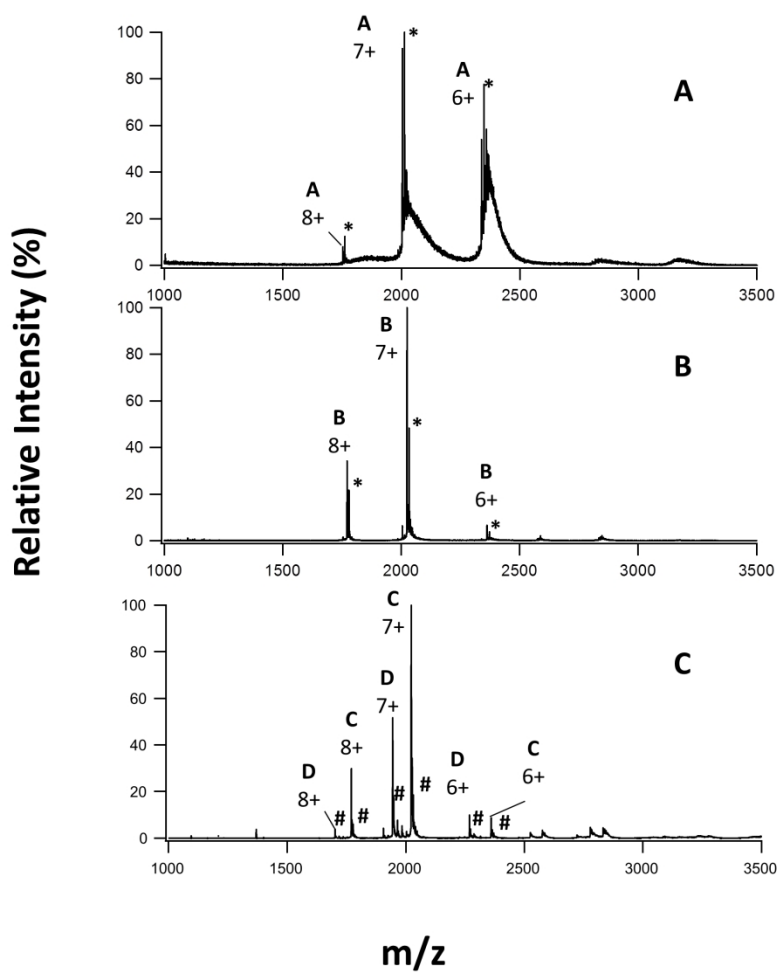


Figure 5

Figure 5

190x254mm (300 x 300 DPI)

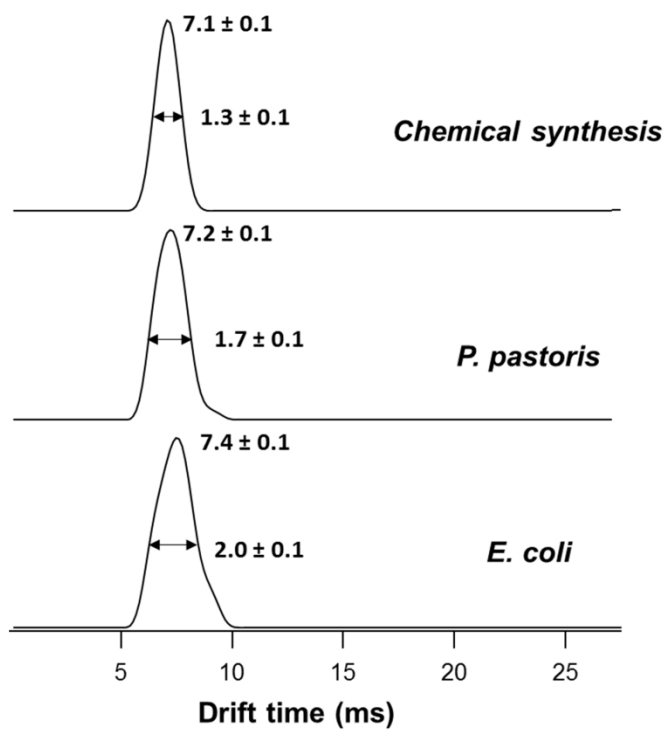


Figure 6

Figure 6

190x254mm (300 x 300 DPI)

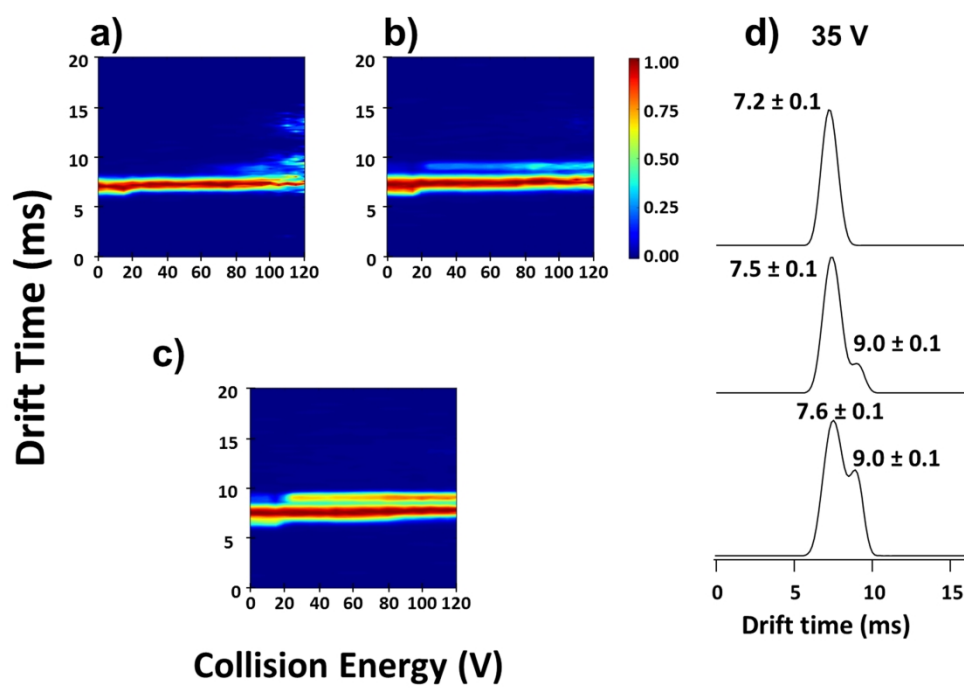


Figure 7

Figure 7

254x190mm (300 x 300 DPI)

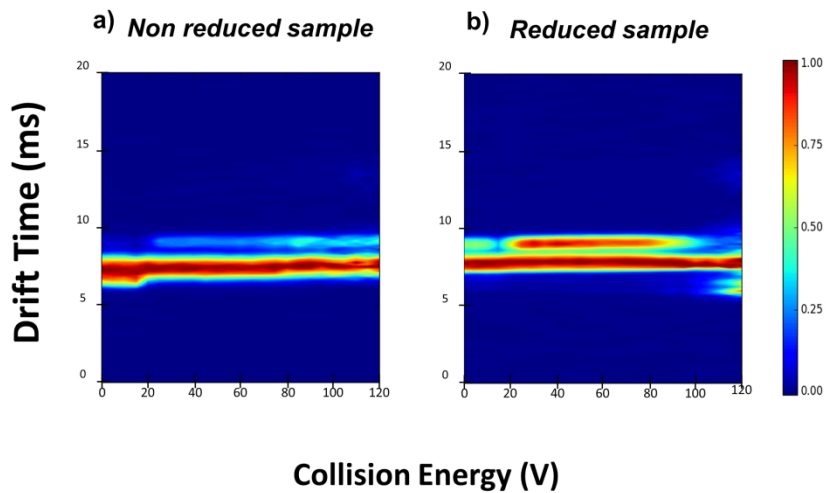


Figure 8

Figure 8

254x190mm (300 x 300 DPI)

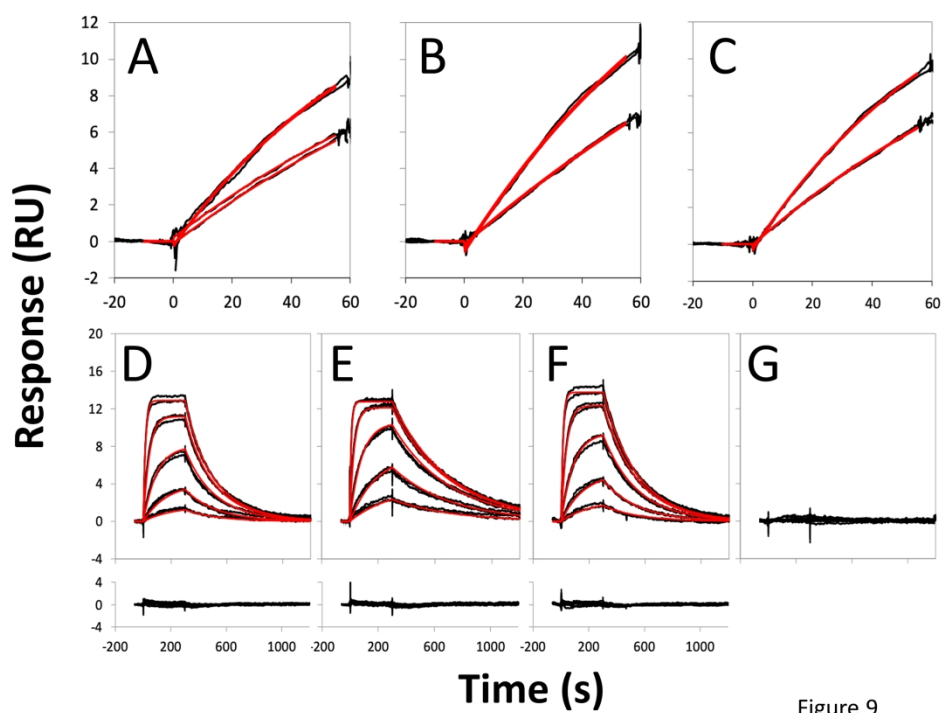


Figure 9

Figure 9

254x190mm (300 x 300 DPI)